



**HAL**  
open science

## Optical diagnosis of gastric tissue biopsies with Mueller microscopy and statistical analysis

Myeongseop Kim, Hee Ryung Lee, Razvigor Ossikovski, Aude Malfait-Jobart, Dominique Lamarque, Tatiana Novikova

► **To cite this version:**

Myeongseop Kim, Hee Ryung Lee, Razvigor Ossikovski, Aude Malfait-Jobart, Dominique Lamarque, et al.. Optical diagnosis of gastric tissue biopsies with Mueller microscopy and statistical analysis. Journal of the European Optical Society : Rapid publications, 2022, 18 (2), pp.10. 10.1051/jeos/2022011 . hal-04537018

**HAL Id: hal-04537018**




**<https://hal.science/hal-04537018>**

Submitted on 8 Apr 2024

**HAL** is a multi-disciplinary open access archive for the deposit and dissemination of scientific research documents, whether they are published or not. The documents may come from teaching and research institutions in France or abroad, or from public or private research centers.

L'archive ouverte pluridisciplinaire **HAL**, est destinée au dépôt et à la diffusion de documents scientifiques de niveau recherche, publiés ou non, émanant des établissements d'enseignement et de recherche français ou étrangers, des laboratoires publics ou privés.

# Optical diagnosis of gastric tissue biopsies with Mueller microscopy and statistical analysis

Myeongseop Kim<sup>1,a</sup>, Hee Ryung Lee<sup>1,a</sup>, Razvigor Ossikovski<sup>1</sup> , Aude Malfait-Jobart<sup>2</sup>, Dominique Lamarque<sup>3</sup> ,  
and Tatiana Novikova<sup>1,4,\*</sup> 

<sup>1</sup> LPICM, CNRS, Ecole Polytechnique, IP Paris, LPICM, Palaiseau 91128, France

<sup>2</sup> Université Paris-Saclay, Université de Versailles St. Quentin-en-Yvelines, INSERM (UMR 1173), Montigny-Le-Bretonneux, France

<sup>3</sup> Université de Versailles St-Quentin en Yvelines, Hôpital Ambroise Paré, Service d'Hépatogastroentérologie,  
Boulogne Billancourt, France

<sup>4</sup> Florida International University, Department of Biomedical Engineering, Miami, FL, USA

Received 28 March 2022 / Accepted 20 October 2022

**Abstract.** We investigate a possibility of producing the quantitative optical metrics to characterize the evolution of gastric tissue from healthy conditions via inflammation to cancer by using Mueller microscopy of gastric biopsies, regression model and statistical analysis of the predicted images. For this purpose the unstained sections of human gastric tissue biopsies at different pathological conditions were measured with the custom-built Mueller microscope. Polynomial regression model was built using the maps of transmitted intensity, retardance, dichroism and depolarization to generate the predicted images. The statistical analysis of predicted images of gastric tissue sections with multi-curve fit suggests that Mueller microscopy combined with data regression and statistical analysis is an effective approach for quantitative assessment of the degree of inflammation in gastric tissue biopsies with a high potential in clinical applications.

**Keywords:** Mueller microscopy, Optical anisotropy, Statistical image analysis, Gastric cancer.

## 1 Introduction

Chronic gastritis is a premalignant condition in a stomach that, if left untreated, favors the development of gastric cancer [1, 2]. Appropriate treatment of chronic gastritis requires precise detection and quantification of gastric mucosa inflammation during medical diagnosis. The gold standard technique is the histology analysis by a pathologist of thin sections of gastric biopsies taken randomly during the endoscopy test [3]. The standard protocol of tissue sections preparation is rather cumbersome and includes many steps (tissue fixation, paraffin embedding, sectioning and staining). Afterward, a pathologist examines prepared thin tissue sections using a white light microscope. Microscopy images of chronic gastritis tissue usually show infiltration of gastric epithelium and lamina propria with the inflammatory cells [4]. In atrophic gastritis the highly differentiated glands, epithelium, and cells are destroyed and replaced by glands and epithelium with immature intestinal properties [5]. However, this histopathology analysis of tissue sections is time-consuming and operator-dependent.

The development of a quantitative metric for the assessment of the degree of gastric inflammation will be beneficial to support the diagnosis of the pathologist [6].

It is known that polarized light is very sensitive to the microstructure of an object under study. The interaction of polarized light beam with a sample changes the polarization state of reflected/transmitted light or even depolarizes it (partially or completely) depending on the optical properties of a sample. Thus, by measuring these modulations or loss of polarization, we may deduce the polarimetric properties (e.g. diattenuation, birefringence, depolarization [7]) of a sample and use them for its characterization. This approach was widely explored in metrological applications [8, 9], food quality control [10–12], pharmaceutical drug studies [13, 14], biomedical diagnosis [15–20], etc. Using changes in tissue depolarization with pathology development for histology analysis and diagnosis was extensively studied in [21–25] for different types of tissue. We suggest using Mueller polarimetric microscopy [26, 27] combined with regression model and statistical analysis of experimental data for the automated quantitative characterization of unstained thin sections of gastric tissue biopsies for the assessment of its degree of inflammation to support pathologist's diagnosis.

\* Corresponding author: [tatiana.novikova@polytechnique.edu](mailto:tatiana.novikova@polytechnique.edu)

<sup>a</sup> Co-first authors.

The basics of Mueller polarimetry, the description of gastric tissue samples, the optical instrument (Mueller Matrix (MM) microscope), and the algorithms of data post-processing (non-linear compression of MM data and regression model for image segmentation) are provided in Section 2. The results of Mueller matrix decomposition, application of the regression model to the microscopy images of total transmitted intensity, linear retardance, dichroism, and depolarization, as well as the statistical analysis of the predicted images are presented and discussed in Section 3. The conclusions of our study are presented in Section 4.

## 2 Methods and materials

### 2.1 Mueller polarimetry

Within the framework of the Stokes–Mueller formalism [7] the polarization of a light beam can be described by a real-valued  $4 \times 1$  Stokes vectors  $S$ . Consequently, the interaction of a polarized light with any linear optical system is described by a following equation:

$$\begin{pmatrix} S'_0 \\ S'_1 \\ S'_2 \\ S'_3 \end{pmatrix} = \begin{pmatrix} M_{00} & M_{01} & M_{02} & M_{03} \\ M_{10} & M_{11} & M_{12} & M_{13} \\ M_{20} & M_{21} & M_{22} & M_{23} \\ M_{30} & M_{31} & M_{32} & M_{33} \end{pmatrix} \begin{pmatrix} S_0 \\ S_1 \\ S_2 \\ S_3 \end{pmatrix}, \quad (1)$$

where the real-valued  $4 \times 4$  Mueller matrix describes the transformation of the input Stokes vector  $S$  into the output Stokes vector  $S'$  upon interaction with a sample. A Stokes vector can describe any polarization state of light (fully or partially polarized), hence, Mueller matrix contains information on the polarimetric properties of any sample (non-depolarizing or depolarizing). Despite the complexity of light-matter interaction process, the polarimetric response of a sample can be expressed in terms of basic polarimetric properties, namely, diattenuation, retardance, and depolarization by performing the decomposition of sample's Mueller matrix. The diattenuation describes the variation of output intensity when changing the probing beam polarization while keeping constant input intensity. Propagation of light through birefringent medium results in different changes of optical phase for the ordinary and extraordinary polarization components. The difference in those phase shifts is called retardance. The depolarization property is characterized by the reduction in degree of polarization of incident beam upon interaction with a sample.

### 2.2 Samples

Thin sections of human gastric tissue with different pathological conditions (control healthy, gastritis, and cancer) were prepared from the random biopsies taken during the standard endoscopy tests. Patients with diagnosed chronic gastritis were enrolled from the cohort GASTRIMED (ClinicalTrials.gov identifier: NCT02325323 [28]) funded

by the French Gastroenterology Society for the studies of link between the gastric mucosa changes in chronic gastritis and the onset of cancer [29]. The patients included in this clinical study (conducted according to the World Medical Association Declaration of Helsinki [30]) were referred to the endoscopic unit of Ambroise Paré Hospital, Boulogne-Billancourt, France. All patients provided their written informed consent (Approval of the Comité de Protection des Personnes Sud-Est III Ethics committee on June 2019, registration number: 19.06.21.76520).

Two adjacent thin tissue sections of  $6 \mu\text{m}$  thickness were prepared for each of three biopsy specimens. One section was stained with hematoxylin and eosin classical protocol (H&E staining) and went through the conventional histology analysis, the gold standard technique for assessing pathological status of tissue. The adjacent unstained gastric tissue section was dewaxed, and its polarimetric properties were measured with a custom-built MM microscope operating in transmission geometry.

### 2.3 Mueller matrix microscope

The detailed description of this instrument is provided elsewhere [31, 32]. For the sake of completeness, we recall the operational principles of the instrument. The custom-built transmission Mueller microscope operates in a visible wavelength range and makes use of the Polarization State Generator (PSG) for the polarization modulation of incident light beam and Polarization State Analyzer (PSA) for the analysis of the polarization state of light beam transmitted by a sample. The PSG is built of a linear polarizer, a quarter wave plate, and two electrically driven ferroelectric liquid crystals and the PSA is composed of the same optical components assembled in a reverse order and placed in the detection arm of the instrument after the microscope objective (Nikon CFI LU Plan Fluor, 20X, Japan). The white light LED (Stemmer Imaging, Germany) was used as a light source and the measurement wavelength of 533 nm was selected by using an interferential filter (spectral bandwidth of 20 nm). Four different polarization states of the incident light beam were generated sequentially by the PSG and projected onto four different polarization states of the PSA after light beam passed through a thin transparent sample. Finally, the light beam was detected by the CCD camera (AV Stingray F-080B, Allied Vision, Germany, image resolution  $600 \times 800$  pixels). The implemented eigenvalue calibration method [33] allows to calculate a  $4 \times 4$  real-valued Mueller matrix (or transfer matrix) of a sample from 16 raw intensity measurements.

### 2.4 Data post-processing

Mueller matrix contains all information on polarization and depolarization properties of a sample; however, the physical interpretation of the elements of Mueller matrix is not always straightforward. We used the differential (or logarithmic) Mueller matrix decomposition (DMMD) method described in [34] for the interpretation of experimental Mueller matrices of thin sections of gastric tissue measured in transmission configuration. This method represents the algorithm of non-linear compression of Mueller matrix

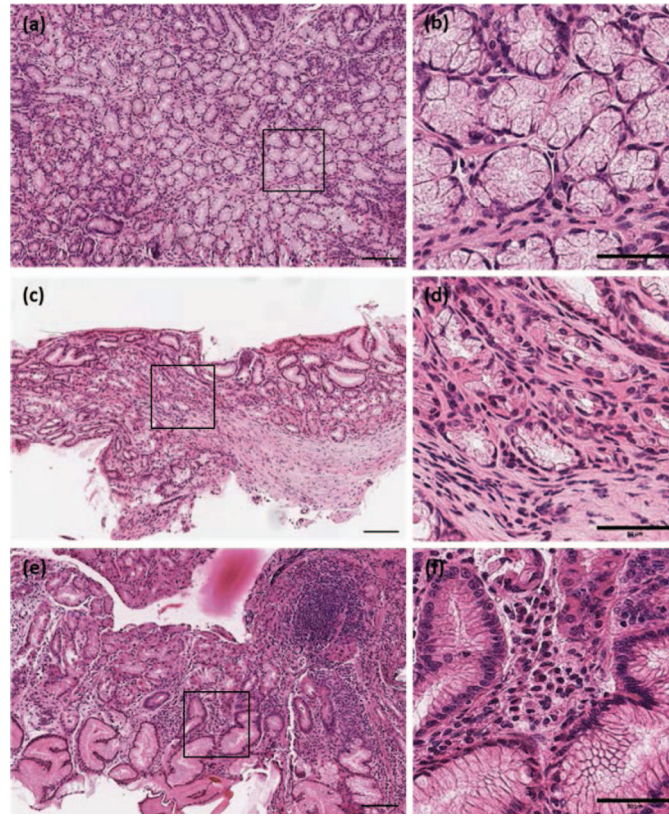


**Fig. 1.** White light microscopy images of H&E stained thin sections of three different human gastric endoscopy biopsies: (a) healthy control (c) chronic gastritis; (e) gastric cancer. The insets (b), (d) and (f) show the enlarged black box zones of the images (a), (c) and (e), respectively. The scale bar is 200  $\mu\text{m}$  in (a), (c) and (e) and 100  $\mu\text{m}$  in (b), (d) and (f).

and is particularly suited for the description of polarimetric properties of biological tissue, because it does not imply the sequential appearance of polarimetric effects, namely, diattenuation, retardation, and depolarization in a sample under study. Assuming that scattering anisotropic medium is homogenous along the trajectory of probing polarized light beam (a reasonable assumption for a few  $\mu\text{m}$  thick tissue section) and applying the DMMD to the recorded Mueller matrix pixel-wise, we obtained the maps of linear and circular dichroism, linear and circular retardance, and depolarization parameters  $\alpha_{22}$ ,  $\alpha_{33}$ , and  $\alpha_{44}$  [26].

Regression analysis is a supervised predictive machine learning approach that evaluates the relation between the independent variables in a given dataset and the dependent variables labelled as the target. There are different types of regression analysis techniques (e.g. linear regression, logistic regression, polynomial regression, etc.) that are applied for data processing [35–39]. For example, the choice of an appropriate algorithm depends on whether a linear or non-linear relationship exists between the target and independent variables.

In our study we applied a polynomial regression model for the diagnostic segmentation of polarimetric images of thin gastric tissue sections [40]. For the sake of completeness we recall the main steps of building such a regression model. We need to define the target value vector  $\vec{Y}$  first. Then we define a training dataset

$X = [\vec{x}_1, \vec{x}_2, \dots, \vec{x}_n]$ . Our primary goal is to calculate the regression model of the target value vector  $\vec{Y}$  from the training dataset  $X$ . In general, a dataset  $X$  depends non-linearly on the target value vector  $\vec{Y}$ . We used the polynomial basis functions of the second degree to create a new feature space  $Z = [1, \vec{x}_1, \vec{x}_2, \dots, \vec{x}_n, \vec{x}_1^2, \vec{x}_2^2, \dots, \vec{x}_n^2]$ . It is necessary to find the solution  $\hat{\beta} = [\beta_0, \beta_1, \dots, \beta_m]^T$  of the following equation:

$$\hat{y} = Z\hat{\beta}, \quad (2)$$

where  $m$  is the dimension of a feature space  $Z$ . We built a regression model by optimizing the mean squared error MSE calculated for the target value vector  $\vec{Y}$  and the predicted value for vector  $\hat{y}$  [41].

$$\begin{aligned} \text{MSE}(\hat{\beta}) &= \frac{1}{N} \sum_{i=1}^N (y_i - \hat{y}_i)^2 = \frac{1}{N} (\vec{Y} - Z\hat{\beta})^T (\vec{Y} - Z\hat{\beta}) \\ &= \frac{1}{N} (\vec{Y}^T \vec{Y} - \vec{Y}^T Z\hat{\beta} - \hat{\beta}^T Z^T \vec{Y} + \hat{\beta}^T Z^T Z\hat{\beta}) \end{aligned} \quad (3)$$

$$\frac{\partial}{\partial \hat{\beta}} (\text{MSE}(\hat{\beta})) = \frac{1}{N} (-Z^T \vec{Y} - Z^T \vec{Y} + (Z^T Z + Z^T Z)\hat{\beta}). \quad (4)$$

To minimize the MSE, we set the derivative to zero and solve for  $\hat{\beta}$ :

$$0 = \frac{1}{N} \left( -2Z^T \vec{Y} + 2Z^T Z \hat{\beta} \right), \quad (5)$$

$$\hat{\beta} = (Z^T Z)^{-1} Z^T \vec{Y}. \quad (6)$$

The elements of vector  $\hat{\beta}$  can be considered as the weight coefficients of the corresponding functions of the feature space  $Z$  that assure the best approximation of the target vector  $\vec{Y}$ .

Then the built regression model with the feature space  $Z$  of training data and the target value vector  $\vec{Y}$  is implemented on the test datasets to generate a predicted image using the feature space  $Z$  of the test dataset and vector  $\hat{\beta}$ .

### 3 Results and discussion

The microscopy images of the H&E stained thin sections of three different types of human gastric endoscopic biopsies: healthy control, chronic gastritis, and gastric cancer tissue are shown in Figure 1. We observe the presence of gastric tissue glands (rounded structures with the mucous cells inside) in the images of healthy control (Figs. 1a and 1b) and chronic gastritis (Figs. 1c and 1d) tissue sections whereas these glands proliferate a lot in cancer (Figs. 1e and 1f). The infiltration of gastric epithelium by inflammatory cells (lymphocytes), already visible in the image of chronic gastritis, becomes very pronounced in the image of gastric cancer tissue. The histology analysis of gastric tissue diagnosis is based on the assessment of these structural differences.

The corresponding adjacent unstained gastric tissue sections were measured with a custom-built MM microscope. The recorded Mueller matrix images were decomposed by applying DMMD and the maps of retardance, diattenuation and depolarization were calculated. Different type of contrast was observed compared to the white light microscopy images. Figure 2 shows the images of total transmitted intensity and scalar retardance measured for all three types of gastric tissue biopsies. The ‘‘honey-comb’’ pattern highlights the zones of optical anisotropy in the images of scalar retardance for both healthy and chronic gastritis tissue. This pattern is related to the presence of fibers in connective tissue forming the walls of gastric gland walls (so-called form birefringence). The zones of higher retardance values in the image of scalar retardance of gastric cancer tissue demonstrate different spatial pattern and reflect the re-arrangement of gastric tissue stroma by malignancy.

Several pixels rendered in red in the images of linear retardance represent high values of these parameters, whereas these pixels are not contrasted in the corresponding transmitted intensity image. The phenomenon of the intranuclear birefringent inclusions (IBI), found in tissue sections prepared using paraffin embedding step, is commonly considered to be a tissue processing artifact. This artifact is related to the presence of residual paraffin left in some cell

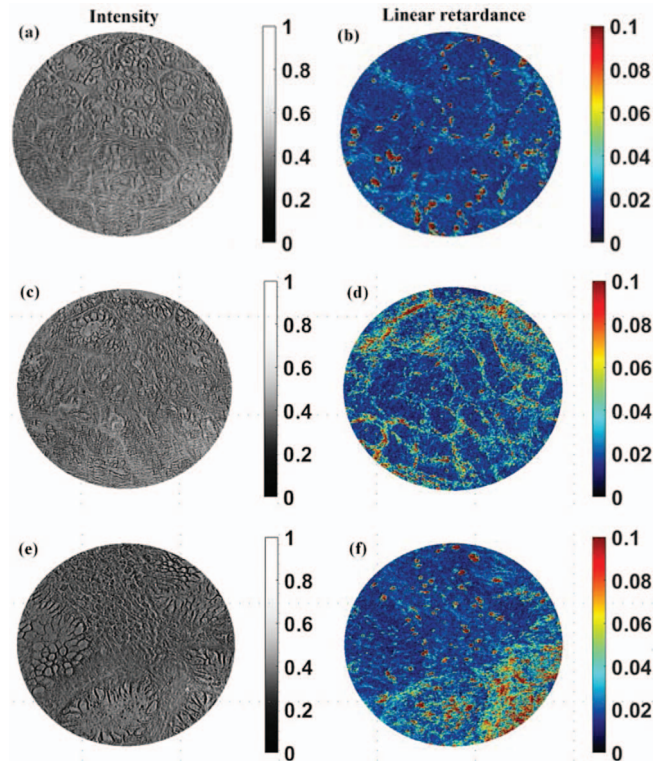


**Fig. 2.** Mueller microscopy images of unstained thin sections of three different human gastric endoscopy biopsies. Normalized transmitted intensity – (a) healthy control, (c) chronic gastritis; (e) gastric cancer. Map of scalar retardance – (b) healthy control, (d) chronic gastritis; (f) gastric cancer. Field of view is about 250  $\mu\text{m}$  in diameter.

nuclei because of insufficient deparaffinization and clearing during tissue processing. Based on the results of [42], we attribute the presence of the pixels which demonstrate high polarimetric values to a paraffin intake by the nuclei of the specific cells. Furthermore, we expect these cells to be the inflammatory ones as they are aligned along the walls of gastric glands [43].

The polynomial regression model was built and applied to generate the predicted microscopic images of unstained thin sections of gastric tissue biopsies recorded with transmission Mueller microscope. First, we selected the region of interest (ROI) to build the regression model. The original image resolution is  $800 \times 600$  pixels, and the selected ROI contains  $400 \times 300$  pixels (see Fig. 3). The training dataset consists of the normalized transmitted intensity image and the maps of the linear retardance, linear dichroism, and circular depolarization calculated by DMMD of the experimental MM images of healthy control gastric tissue section. Based on this information, we look for the efficient image segmentation algorithm to increase the contrast between the zones of connective tissues and gastric tissue glands in order to produce the quantitative metrics for gastric tissue diagnosis.

As was mentioned above, it is required to set the target image because the data regression technique is a supervised machine learning algorithm. The pixels corresponding to

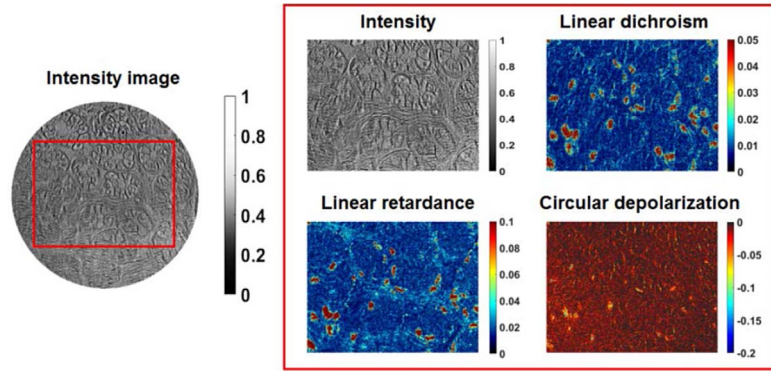


**Fig. 3.** Selection of the region of interest (red box –  $400 \times 300$  pixels, left panel) and corresponding training dataset (size of  $4 \times 400 \times 300$ ) – the images of transmitted intensity, linear retardance, linear dichroism, and circular depolarization of healthy control gastric tissue.

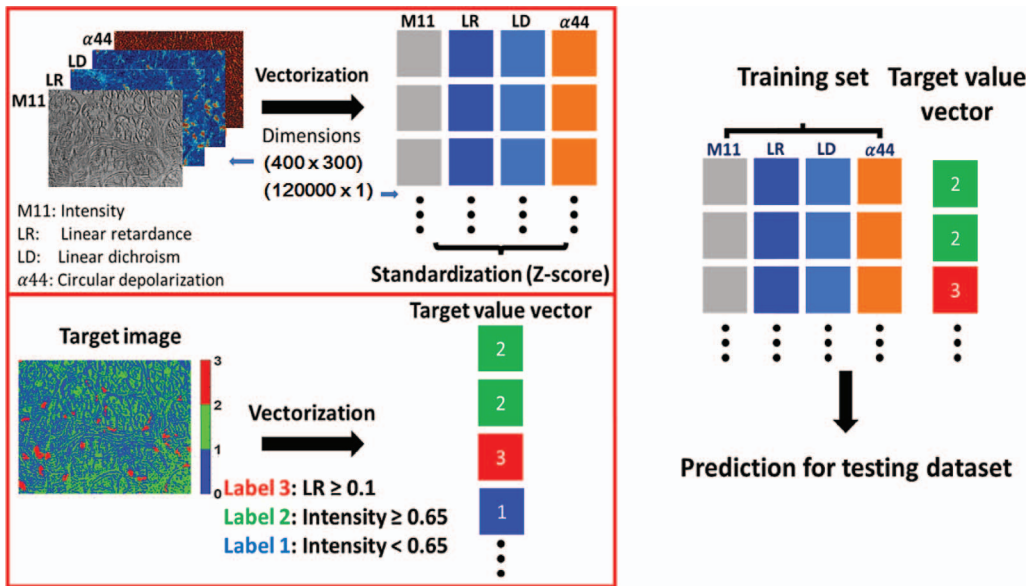


**Fig. 4.** The main steps of building the regression model using training set of the intensity and polarimetric images of healthy control gastric tissue section.

the linear retardance values  $>0.1$  radians were tagged with the label 3. It is worth to note that those pixels also demonstrate large value of dichroism and large absolute value of depolarization. Since the glands and the mucus cells within the glands have similar optical properties, the pixels with the normalized intensity values  $> 0.65$  were tagged with the label 2 in the target image. The remaining pixels were tagged with the label 1. The defined target image demonstrates the enhanced contrast between the connective tissue and zones with large polarimetric values (see Fig. 4, left bottom panel).

Then the polynomial regression model described by equations (2)–(6) was constructed based on this target image, and applied to the testing datasets (polarimetric images of chronic gastritis and gastric cancer sections) for the automated image processing and diagnostic segmentation. The main steps of building the regression model are

illustrated in Figure 4. First, we apply the vectorization of training images of the normalized transmitted intensity M11, linear dichroism LD, linear retardance LR and circular depolarization  $\alpha_{44}$  of healthy control gastric tissue section in order to transform each  $400 \times 300$  matrix into a  $120\,000 \times 1$  vector. The data standardization (so-called z-score) is required to account for different vectors' units [44]. The vectorization was also applied to the target image. Based on this training set and the target vector values, we calculate the coefficients of the polynomial regression model as was described in Section 2. We used the polynomial basis functions of the second degree to avoid overfitting. The training step for the selected dataset of the size of  $4 \times 400 \times 300$  took 2.73 s using the computer with the processor Intel(R) Core(TM) i5-8265U CPU @ 1.60 GHz and 16.0 GB of RAM. The polynomial regression model was further used on the testing sets of polarimetric images

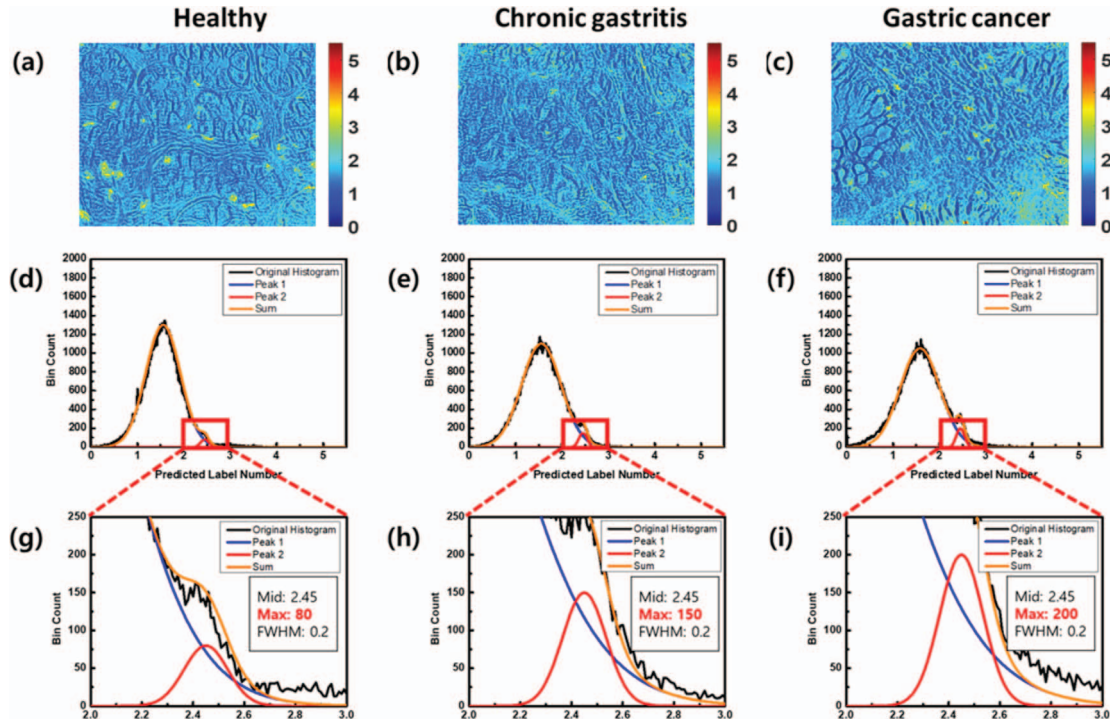


**Fig. 5.** Predicted images ( $400 \times 300$  pixels) of gastric tissue sections: (a) healthy, (b) chronic gastritis, (c) gastric cancer), (d–f) histograms of the corresponding predicted images; (g–i) insets with the enlarged view of the second Gaussian peak.

of chronic gastritis and gastric cancer sections to generate the corresponding predicted images.

The prediction of the regression model for the healthy control gastric tissue section is shown in Figure 5 (top row, left panel). The connective tissue and mucus cells are clearly visible as well as the zones that correspond to the large values of linear retardance.

We also applied the regression model trained on the images of healthy control tissue sections to the images of chronic gastritis (Fig. 5a) and gastric cancer (Fig. 5b) tissue sections. The connective tissue of gland walls is distinguishable in the predicted image for chronic gastritis, whereas all glands are erased in the predicted image of cancerous gastric tissue (Fig. 5c). The zones with large values of scalar retardance are still present in the predicted images of both chronic gastritis and gastric cancer biopsies.

We performed two Gaussians fit to the histograms of predicted image values for three different types of the gastric samples (e.g. healthy, chronic gastritis, and gastric cancer) to compare them quantitatively. We focus on the analysis of the position, width and height of the Gaussian peaks. The parameters of a first Gaussian do not demonstrate significant variation with pathological status of gastric tissue. The position of second peak and its full width at half maximum (FWHM) also do not show strong variations, being 2.45 and 0.2, respectively. On the contrary, the height of a second Gaussian increases for chronic gastritis and cancerous gastric tissue sections compared to healthy gastric tissue. The value of height of a second peak is equal to 80 for healthy control gastric tissue. This value increases up to 150 (almost twice) for the chronic gastritis tissue and

becomes equal to 200 for gastric cancer tissue. We suggest using this parameter as a quantitative metric for unstained gastric tissue section diagnosis in order to provide an accurate grading of gastric tissue inflammation to support pathologist's analysis.

## Conclusions

The ultimate goal of this study is the development of the procedure for an automated fast analysis of the polarimetric images of thin unstained sections of gastric tissue biopsies for tissue diagnosis (i.e., detection of different pathology conditions: gastric cancer, inflammation, gastritis and its quantification). For this purpose, we have implemented and tested an automated image processing algorithm based on the regression model of intensity, total scalar retardance, and depolarization images obtained with MM microscopy for gastric tissue diagnosis to support the gold standard analysis by a pathologist. The polynomial regression model was implemented for the image segmentation. Further, the statistical analysis of the predicted images was performed by a two-Gaussian fit to provide the quantitative metrics for gastric tissue diagnosis. The height of a second Gaussian peak was shown to be sensitive to the pathological status of measured sample, thus, holding the promise to become a quantitative metric for the digital histology analysis. It is worth to mention that the suggested approach does not require tissue staining and, thus, can reduce the time of tissue section preparation.

The perspectives for future studies include the gold standard histology analysis of the pathological status of high-paraffin intake cells. We expect the high value of scalar retardance for the high-paraffin intake cells to be a possible marker of the inflammatory cells. The statistical analysis of the predicted images has to be performed on a larger dataset of gastric tissue biopsies at different health conditions to test the detection performance of optical polarimetric diagnosis and estimate the variability and standard deviation of the suggested metrics of tissue pathological status. It will be the subject of our subsequent studies.

The obtained results suggest that Mueller-matrix polarimetry can be an effective approach for screening optical anisotropy variations in tissue-like highly scattering media, with a high potential in clinical application for diagnosis of cancerous tissues. Using thick blocks of excised tissue for the preliminary optical analysis by pathologist may considerably reduce the time and cost of diagnostics. To capitalize on our initial findings the measurements and statistical, correlation and fractal analysis of larger number of paraffin-embedded tissue samples will be undertaken in a future work.

## Declarations

### Availability of data and material

Data underlying the results presented in this paper are not publicly available at this time but may be obtained from the authors upon reasonable request.

### Competing interests

The authors declare that they have no competing interests.

### Authors' contributions

Myeongseop Kim: Software, Formal analysis, Writing – Original draft preparation; Hee Ryung Lee: Investigation, Visualization, Data Curation, Writing – Original draft preparation; Aude Malfait-Jobart: Data curation, Validation, Visualization; Razvigor Ossikovski: Methodology; Dominique Lamarque: Investigation, Resources, Validation; Tatiana Novikova: Conceptualization, Methodology, Supervision, Writing – Reviewing and Editing.

## References

- Sipponen P. (1989) Atrophic gastritis as a premalignant condition, *Ann. Med.* **21**, 4, 287–290.
- Genta R.M., Rugge M. (2006) Assessing risks for gastric cancer: New tools for pathologists, *World J. Gastroenterol.* **12**, 35, 5622–5627.
- Carpenter H.A., Talley N.J. (1995) Gastroscopy is incomplete without biopsy: clinical relevance of distinguishing gastropathy from gastritis, *Gastroenterology* **108**, 917–924.
- Correa P., Piazuelo B. (2012) The gastric precancerous cascade, *J. Dig. Dis.* **13**, 1, 2–9.
- Sipponen P., Maaros H.I. (2015) Chronic gastritis, *Scand. J. Gastroenterol.* **50**, 6, 657–667.
- Baxi V., Edwards R., Montalto M., Saha S. (2022) Digital pathology and artificial intelligence in translational medicine and clinical practice, *Mod. Pathol.* **35**, 23–32.
- Goldstein D.H. (2010) *Polarized light*, 3rd edn., CRC Press.
- Novikova T., Bulkin P. (2021) Inverse problem of Mueller polarimetry for metrological applications, *J. Inverse Ill-Posed Probl.* **29**, 5, 759–774.
- Kaplan B., Novikova T., De Martino A., Drévilion B. (2004) Characterization of bidimensional gratings by spectroscopic ellipsometry and angle-resolved Mueller polarimetry, *Appl. Opt.* **43**, 6, 1233–1240.
- Sarkar M., Gupta N., Assaad M. (2019) Monitoring of fruit freshness using phase information in polarization reflectance spectroscopy, *Appl. Opt.* **58**, 23, 6396–6405.
- Peyvasteh M., Popov A., Bykov A., Pierangelo A., Novikova T., Meglinski I. (2021) Evolution of raw meat polarization-based properties by means of Mueller matrix imaging, *J. Biophotonics* **4**, 15, e202000376.
- Blokhina A.A., Ryzhova V.A., Korotaev V.V., Kleshchenok M.A. (2017) The meat product quality control by a polarimetric method, *Proc. SPIE Medical Applications of Laser-Generated Beams of Particles IV: Review of Progress and Strategies for the Future* **10239**, 102390K.
- Brullot W., Vanbel M.K., Swusten T., Verbiest T. (2016) Resolving enantiomers using the optical angular momentum of twisted light, *Sci. Adv.* **2**, 3, e1501349.
- Sugano K., Kato T., Suzuki K., Keiko K., Sujaki T., Mano T. (2006) High throughput solubility measurement with automated polarized light microscopy analysis, *J. Pharm. Sci.* **95**, 10, 2115–2122.
- Chue-Sang J., Holness N., Gonzalez M., Greaves J., Saytashev I., Stoff S., Gandjbakhche A., Chernomordik V.V., Burkett G., Ramella-Roman J.C. (2018) Use of Mueller matrix colposcopy in the characterization of cervical collagen anisotropy, *J. Biomed. Opt.* **23**, 12, 1–9.
- Schucht P., Lee H.R., Mezouar M.H., Hower E., Raabe A., Murek M., Zubak I., Goldberg J., Kovari E., Pierangelo A., Novikova T. (2020) Visualization of white matter fiber tracts of brain tissue sections with wide-field imaging Mueller polarimetry, *IEEE Trans. Med. Imaging* **39**, 12, 4376–4382.
- Beer F., Wartak A., Pircher N., Holzer S., Lammer J., Schmidinger G., Baumann B., Pircher M., Hitzinger C.K. (2018) Mapping of corneal layer thicknesses with polarization-sensitive optical coherence tomography using a conical scan pattern, *Invest. Ophthalmol. Vis. Sci.* **59**, 5579–5588.
- Borovkova M., Bykov A., Popov A., Pierangelo A., Novikova T., Pahnke J., Meglinski I. (2020) Evaluating  $\beta$ -amyloidosis Progression in Alzheimer's Disease with Mueller Polarimetry, *Biomed. Opt. Express* **11**, 8, 4509–4519.
- Ivanov D., Dremmin V., Bykov A., Borisova E., Genova T., Popov A., Ossikovski R., Novikova T., Meglinski I. (2020) Colon cancer detection via Poincaré sphere representation and 2D polarimetric mapping of ex vivo colon sample, *J. Biophotonics* **13**, 8, e202000082.
- He H., Sun M., Zeng N., Du E., Liu S., Guo Y., Wu J., He Y., Ma H. (2014) Mapping local orientation of aligned fibrous scatterers for cancerous tissues using backscattering Mueller matrix imaging, *J. Biomed. Opt.* **19**, 10, e202000082.
- Ushenko V.A., Hogan B.T., Dubolazov A., Grechina A.V., Boronikhina T.V., Gorsky M., Ushenko A.G., Ushenko Y.O., Bykov A., Meglinski I. (2021) Embossed topographic depolarisation maps of biological tissues with different morphological structures, *Sci. Rep.* **11**, 3871.



- 22 Ushenko V.A., Hogan B.T., Dubolazov A., Piavchenko G., Kuznetsov S.I., Ushenko A.G., Ushenko Y.O., Gorsky M., Bykov A., Meglinski I. (2021) 3D Mueller matrix mapping of layered distributions of depolarisation degree for analysis of prostate adenoma and carcinoma diffuse tissues, *Sci. Rep.* **11**, 5162.
- 23 Trifonyuk L., Sdobnov A., Baranowski W., Ushenko V., Olar O., Dubolazov A., Pidkamin L., Sidor M., Vanchuliak O., Motrich A., Gorsky M., Meglinski I. (2020) Differential Mueller matrix imaging of partially depolarizing optically anisotropic biological tissues, *Lasers Med. Sci.* **35**, 877–891.
- 24 Peyvaste M., Dubolazov A., Popov A., Ushenko A., Ushenko Y., Meglinski I. (2020) Two-point Stokes vector diagnostic approach for characterization of optically anisotropic biological tissues, *J. Phys. D: Appl. Phys.* **53**, 395401.
- 25 Borovkova M., Trifonyuk L., Ushenko V., Dubolazov A., Vanchulyak O., Bodnar G., Ushenko Y., Olar O., Ushenko A., Sakhnovskiy M., Bykov A., Meglinski I. (2019) Mueller-matrix-based polarization imaging and quantitative assessment of optically anisotropic polycrystalline networks, *PLoS ONE* **14**, 5, e0214494.
- 26 Lee H.R., Yoo T.S.H., Li P., Lotz C., Kai Groeber-Becker F., Dembski S., Garcia-Cauarel E., Ossikovski R., Novikova T. (2018) Mueller microscopy of anisotropic scattering media: theory and experiments, *Proc. SPIE Unconventional Optical Imaging* **10677**, 1067718.
- 27 Li P., Lee H.R., Chandel S., Lotz C., Kai Groeber-Becker F., Dembski S., Ossikovski R., Ma H., Novikova T. (2020) Analysis of tissue microstructure with Mueller microscopy: logarithmic decomposition and Monte Carlo modeling, *J. Biomed. Opt.* **25**, 1, 015002.
- 28 GASTRIMED (2014) *Prognosis and risk factors of gastric cancer in patients with intestinal metaplasia*. <https://clinicaltrials.gov/ct2/show/NCT02325323>.
- 29 Bazin T., Martinez-Herrera S.E., Jobart-Malfait A., Benzeeth Y., Boffety M., Julié C., Emile J.F., Michel V., Goudail F., Touati E., Marzani F., Lamarque D. (2020) Multispectral imaging detects gastritis consistently in mouse model and in humans, *Sci. Rep.* **10**, 20047.
- 30 World Medical Association. *WMA Declaration of Helsinki – Ethical principles for medical research involving human subjects*. <https://www.wma.net/policies-post/wma-declaration-of-helsinki-ethical-principles-for-medical-research-involving-human-subjects/>.
- 31 Lee H.R., Li P., Yoo T.S.H., Lotz C., Kai Groeber-Becker F., Dembski S., Garcia-Cauarel E., Ossikovski R., Ma H., Novikova T. (2019) Digital histology with Mueller microscopy: how to mitigate an impact of tissue cut thickness fluctuations, *J. Biomed. Opt.* **24**, 7, 076004.
- 32 Lee H.R., Saytashev I., Du Le V.N., Mahendroo M., Ramella-Roman J.C., Novikova T. (2021) Mueller matrix imaging for collagen scoring in mice model of pregnancy, *Sci. Rep.* **11**, 1, 15621.
- 33 Compain E., Poirier S., Drevillon B. (1999) General and self-consistent method for the calibration of polarization modulators, polarimeters, and Mueller-matrix ellipsometers, *Appl. Opt.* **38**, 16, 3490–3502.
- 34 Gil-Perez J.J., Ossikovski R. (2016) *Polarized Light and the Mueller Matrix Approach*, CRC Press.
- 35 Schneider A., Hommel G., Blettner M. (2010) Linear regression analysis: part 14 of a series on evaluation of scientific publications, *Dtsch. Arztebl. Int.* **107**, 44, 776–782.
- 36 Silhavy R., Silhavy P., Prokopova Z. (2017) Analysis and selection of a regression model for the use case points method using a stepwise approach, *J. Syst. Softw.* **125**, 1–14.
- 37 Prabhakar T.V.N., Xavier G., Geetha P., Soman K. (2015) Spatial preprocessing based multinomial logistic regression for hyperspectral image classification, *Procedia Comput. Sci.* **46**, 1817–1826.
- 38 Baseer K.K., Neerugatti V., Tatekalva S., Babu A.A. (2019) Analysing various regression models for data processing, *Int. J. Innov. Technol. Exploring Eng.* **8**, 731–736.
- 39 Witten I.H., Frank E., Hall M.A. (2011) *Data mining: practical machine learning tools and techniques*, 3rd edn., Elsevier Inc.
- 40 Lo Vercio L., Amador K., Bannister J.J., Crites S., Gutierrez A., MacDonald M.E., Moore J., Mouches P., Rajashekar D., Schimert S., Subbanna N., Tuladhar A., Wang N., Wilms M., Winder A., Forkert N.D. (2020) Supervised machine learning tools: a tutorial for clinicians, *J. Neural. Eng.* **17**, 062001.
- 41 Akdeniz F., Erol H. (2003) Mean squared error matrix comparisons of some biased estimators in linear regression, *Commun. Stat. Theory Methods* **32**, 12, 2389–2413.
- 42 Vitkunaite A., Laurinaviciene A., Plancoulaine B., Rasmusson A., Levenson R.M.S., Laurinavicius A. (2021) Intracellular birefringent inclusions in paraffin sections by polychromatic polarization microscopy, *Sci. Rep.* **11**, 6275.
- 43 Pennelli G., Grillo F., Galuppini F., Ingravallo G., Pillozzi E., Rugge M., Fiocca R., Fassan M., Mastracci L. (2020) Gastritis: update on etiological features and histological practical approach, *Pathologica* **112**, 3, 153–165.
- 44 Roessner U., Nahid A., Chapman B., Hunter A., Bellgard M. (2011) Metabolomics – the combination of analytical biochemistry, biology and informatics, in: *Scientific Fundamentals of Biotechnology*, Vol. **1**, 2nd edn, Elsevier, 447 p.